Article

Synthesis and Electrocatalytic Performance of Multi-Component Nanoporous PtRuCuW Alloy for Direct Methanol Fuel Cells

Xiaoting Chen [1],[†], Hao Wang [1],[†], Ying Wang [1], Qingguo Bai [1], Yulai Gao [2] and Zhonghua Zhang [1],*

[1] Key Laboratory for Liquid-Solid Structural Evolution and Processing of Materials (Ministry of Education), School of Materials Science and Engineering, Shandong University, Jingshi Road 17923, Jinan 250061, China; E-Mails: sdu12chxt@gmail.com (X.C.); beishangdehonghu@163.com (H.W.); wy18766311718@163.com (Y.W.); baychrist@163.com (Q.B.)

[2] Laboratory for Microstructures, Shanghai University, 99 Shangda Road, Shanghai 200436, China; E-Mail: ylgao@shu.edu.cn

[†] These authors contributed equally to this work.

* Author to whom correspondence should be addressed; E-Mail: zh_zhang@sdu.edu.cn; Tel./Fax: +86-531-88396978.

Abstract: We have prepared a multi-component nanoporous PtRuCuW (np-PtRuCuW) electrocatalyst via a combined chemical dealloying and mechanical alloying process. The X-ray diffraction (XRD), transmission electron microscopy (TEM) and electrochemical measurements have been applied to characterize the microstructure and electrocatalytic activities of the np-PtRuCuW. The np-PtRuCuW catalyst has a unique three-dimensional bi-continuous ligament structure and the length scale is 2.0 ± 0.3 nm. The np-PtRuCuW catalyst shows a relatively high level of activity normalized to mass (467.1 mA mg_{Pt}^{-1}) and electrochemically active surface area (1.8 mA cm^{-2}) compared to the state-of-the-art commercial PtC and PtRu catalyst at anode. Although the CO stripping peak of np-PtRuCuW 0.47 V (*vs.* saturated calomel electrode, SCE) is more positive than PtRu, there is a 200 mV negative shift compared to PtC (0.67 V *vs.* SCE). In addition, the half-wave potential and specific activity towards oxygen reduction of np-PtRuCuW are 0.877 V (*vs.* reversible hydrogen electrode, RHE) and 0.26 mA cm^{-2}, indicating a great enhancement towards oxygen reduction than the commercial PtC.

1. Introduction

In recent decades, there are increasing requirements for high-efficiency and eco-friendly energy to cope with environment problems, such as the depletion of energy and pollution. Direct methanol fuel cells (DMFCs) meet the above requirement and are important for the automotive industry [1,2]. As an important component, the state-of-the-art electrocatalysts must ensure the methanol oxidation reaction (MOR) at anode and oxygen reduction reaction (ORR) at cathode to generate electricity with water and carbon dioxide as the byproducts [1,3]. The use of current catalysts has several disadvantages including the low catalytic efficiency as well as CO tolerance, and sluggish kinetics towards ORR. Much effort has been dedicated to alloying Pt with other metals (e.g., Fe [4], Co [5–7], Ni [5,8,9], Cu [10], Sn [11], *etc.*) to improve electrochemical activities. For high-activity applications of DMFCs, PtRu alloy remains the most active electrocatalyst due to its unique reaction mechanism [12,13]. Based upon the bi-functional and electronic effects [14–16], the electrocatalytic performance of catalysts could be significantly enhanced through compositional design of catalysts. For instance, W/Mo-modified PtRu/C showed improved electro-oxidation activity in comparison to the un-modified PtRu/C [17]. The PtRuOsIr showed better activity compared to PtRuOs and PtRuIr [3].

Traditional preparation methods for Pt-based alloys have been focusing on microemulsions [18,19], microwave irradiation [20], electrodeposition [21] and chemical reduction [3,22]. These processes are limited to the tunability of alloy composition, cockamamie, and not suitable for batch production, which hampers the commercialization of DMFCs. Thus, although there are obvious advantages in multicomponent catalysts, most of the prior studies were restricted to the synthesis of binary and ternary alloys. In contrast, facile dealloying has shown its advantage in preparing nanoporous metals/alloys. Thus, materials with unique nanoporous structure possess intriguing physical and chemical properties to generate promising potentials for various important applications such as sensors [23], mechanical actuators [24] and catalysis [25,26].

From the viewpoint of activity and accessibility, Cu are W are superior candidates as indispensible component in catalysts. In previous work, PtRuCu [27,28] and PtRuW [29,30] ternary alloys have received unremitting interest. As part of the continuing effort in new catalyst exploration, the nanoporous PtRuCuW (np-PtRuCuW) alloy was synthesized through mechanical alloying and subsequent mild chemical dealloying process in the present paper. This new catalyst was characterized with electrochemical measurements at the anode as well as cathode for DMFCs. Our results show that the np-PtRuCuW catalyst performs better than the commercial PtC and PtRu catalysts. Furthermore, the catalyst can be synthesized in gram-scale, which makes repeatable experiments in laboratory possible and batch preparation in factory reliable. Given the advantages, including easy access to component design, simplicity in the fabrication process and the enhanced activity, we hope that the combination of mechanical alloying with dealloying provides an efficient way to design multicomponent catalyst materials.

2. Results and Discussion

2.1. Microstructural Characterization of np-PtRuCuW

Figure 1 shows the X-ray diffraction (XRD) patterns of the $Al_{66}Cu_{30}(Pt_{53}Ru_{32}W_{15})_4$ precursor alloy and the as-dealloyed samples. In Figure 1a, a number of diffraction peaks appear on the pattern of the as-milled $Al_{66}Cu_{30}(Pt_{53}Ru_{32}W_{15})_4$ precursor, which can be ascribed to a Al_4Cu_9-type (PDF No. 65-3347) intermetallic phase and Ru (PDF No. 06-0663). In addition, there is a sharp peak around scattering angles (2θ) of *ca.* 40° which can be ascribed to PtRu. A little amount of Ru dissolved during the dealloying process, leading to the reduction of peak intensity and increase of peak width around 40° [31]. The XRD spectrum presents obviously broadened Bragg peaks at scattering angles (2θ) of *ca.* 40.8°, 47.1° and 69.4° (Figure 1b) compared to the precursor alloy. These signals consist with the face-centered cubic (f.c.c.) Pt (PDF No. 04-0802) in spite of the shifting of Bragg peaks. In addition, the Ru diffraction peaks still exist after dealloying (Figure 1b). Due to the minor addition of Ru (only 1.28 at %) into the precursor, the strong diffraction peaks of Ru also suggest the alloying of other elements (Pt, W and Al) with Ru to form a solid solution. Also, it is understandable to assume that the alloying of Pt with Ru as well as Cu and W results in the shift towards higher Bragg angles [32]. The chemical component of the as-dealloyed samples was characterized by EDX and one typical spectrum is presented in Figure 1c. The corresponding results reveal that the sample is composed of Pt (56.2 at %), Ru (18.7 at %), Cu (14.2 at %) and W (10.9 at %), with a minor residual Al (only few atom percent) could be detected in the as-dealloyed samples.
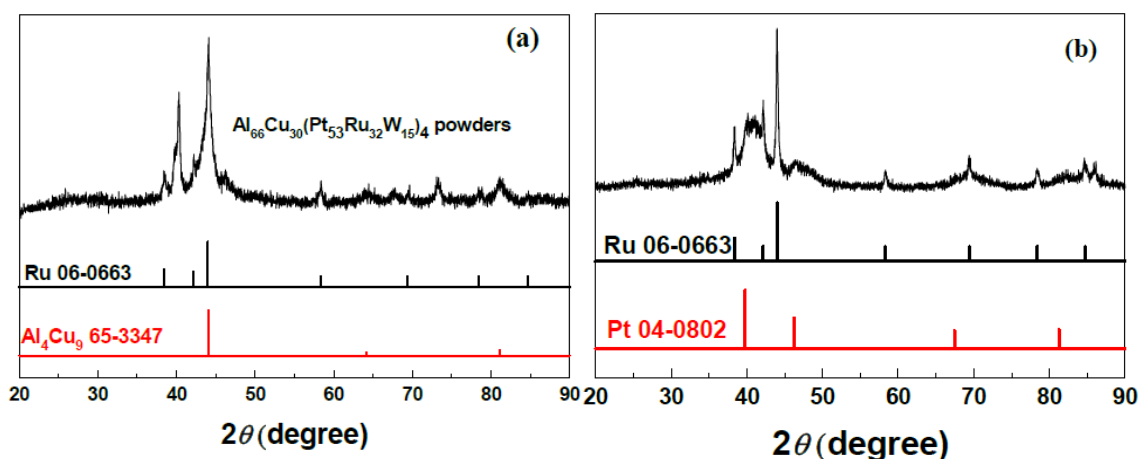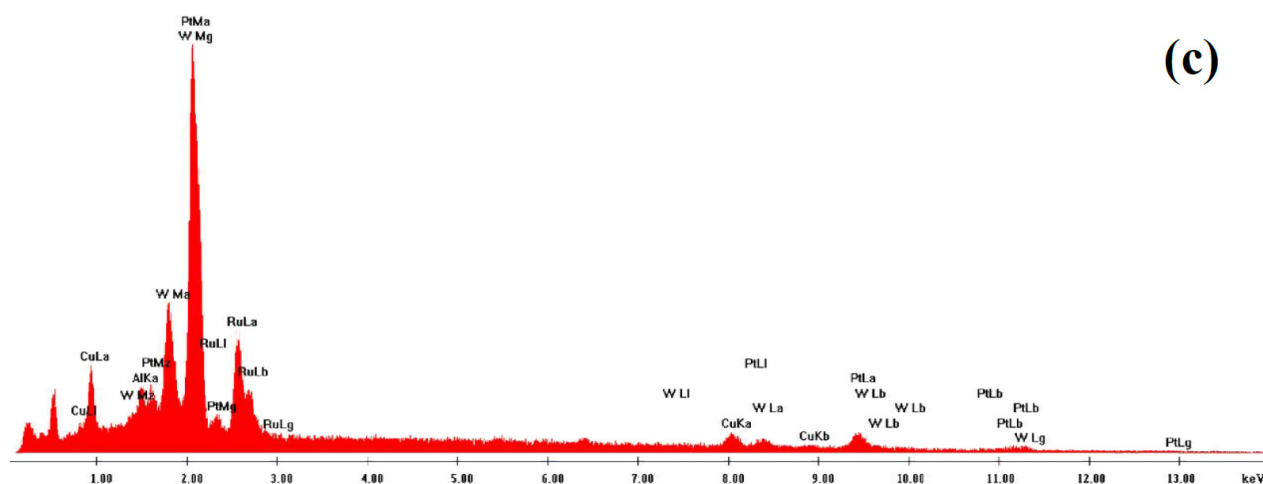

Figure 1. *Cont.*

(c)

Figure 1. XRD spectrum of (**a**) the mechanically alloyed $Al_{66}Cu_{30}(Pt_{53}Ru_{32}W_{15})_4$ powders; (**b**) the precursor alloy after dealloying in the 1M HNO_3 solution; and (**c**) corresponding EDX result of the as-dealloyed samples.

As shown in Figure 2a,b, the final samples display a nanoporous structure composed of interconnected nanoscaled ligaments (2.0 ± 0.3 nm in size) and bi-continuous channels. Besides the ultrafine ligament/channel structure, nanoparticles embedded in the nanoporous matrix are observed, and one particle is marked by a red arrow in Figure 2b. The unique nanostructure results from the dealloying process and similar phenomenon has been studied before [33,34]. The diffraction rings come from the nanoporous matrix and correspond to (111), (200), (220) and (311) reflections of f.c.c. Pt and the diffraction spots originate from the embedded nanoparticles corresponding to the Ru phase (inset of Figure 2a). Overall, the transmission electron microscopy (TEM) results are consistent with the XRD results from Figure 1b.

The high-resolution TEM (HRTEM) images show typical bi-continuous ligament-channel structure of the as-dealloyed samples (Figure 2c,d). The ligaments are composed of small nanocrystals of several nanometers and the spacing of some lattice fringes is 0.222 nm (as indicated in Figure 2d), which is similar to the (111) crystal plane of f.c.c. Pt (~0.226 nm). The corresponding fast Fourier transform (FFT) pattern further verifies the nanocrystalline character of the selected area (presented in the inset of Figure 2d). In addition, Figure 2d also shows the HRTEM image of another area. The lattice spacing of these regular lattice fringes running across the area is 0.232 nm, which is close to the value of Ru (100) crystal plane (0.234 nm). Both the XRD and TEM results confirm that partial Ru failed to be alloyed with Pt and the final as-dealloyed samples include Ru and Pt solid solution. The np-PtRuCuW can be used as abbreviation for the obtained samples.
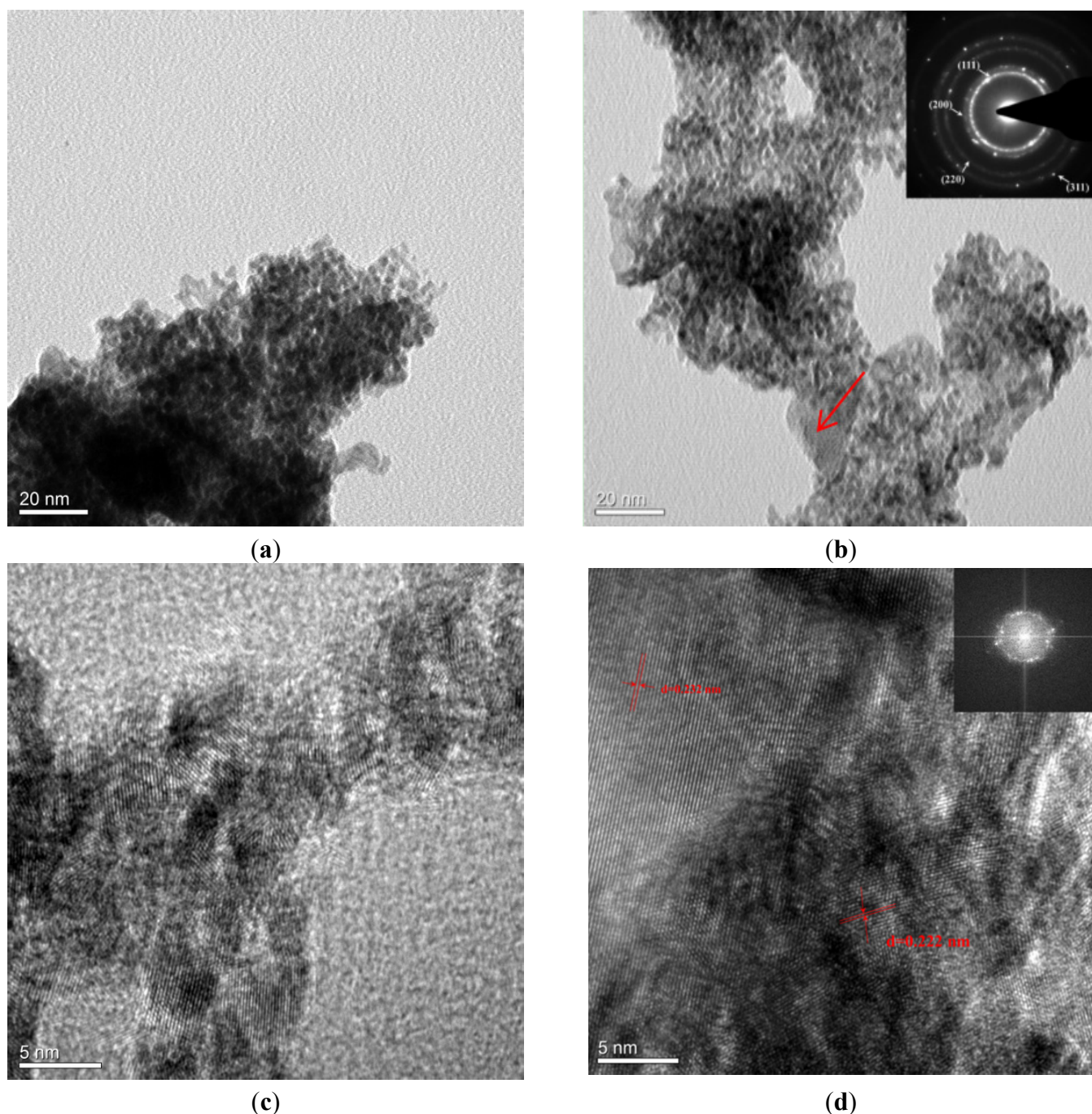
Figure 2. (**a**,**b**) TEM and (**c**,**d**) HRTEM images of the np-PtRuCuW alloy with nanoporous microstructure; Insets in (**b**,**d**): typical SAED and FFT spectrums, respectively.

2.2. Catalytic Activity of np-PtRuCuW at Anode

The activation step results in the catalyst surface cleaning and typical electrochemical features including the typical hydrogen ad/desorption, double layer and metallic redox region [35]. In addition, less-noble metals dissolution would happen when applying potential cycling to multi-metallic alloys [32,36,37]. For np-PtRuCuW, the CV features are different from the PtC and PtRu catalysts (Figure 3a). Firstly, there are broader double electric layer and a more featureless shoulder region than PtC. Moreover, the reduction peak of Pt oxides shifts to a more positive direction compared to the PtC and PtRu catalysts (as highlighted by dotted line in Figure 3a). The characteristics are typical to

multi-component alloys [7,27,32,36,37]. Normally, the electrochemically active surface area (ECSA) can be obtained from the equation $ECSA_{Pt}$ (m²/g) = $Q_H/(2.1 \times m_{Pt})$ by integrating the hydrogen ad/desorption charge and using the value of 2.1 C m^{-2} for the oxidation of a monolayer of hydrogen on a polycrystalline Pt electrode [35,38]. The ECSAs of the np-PtRuCuW, PtC and PtRu catalysts were determined to be 26, 47 and 40 m² g^{-1}.
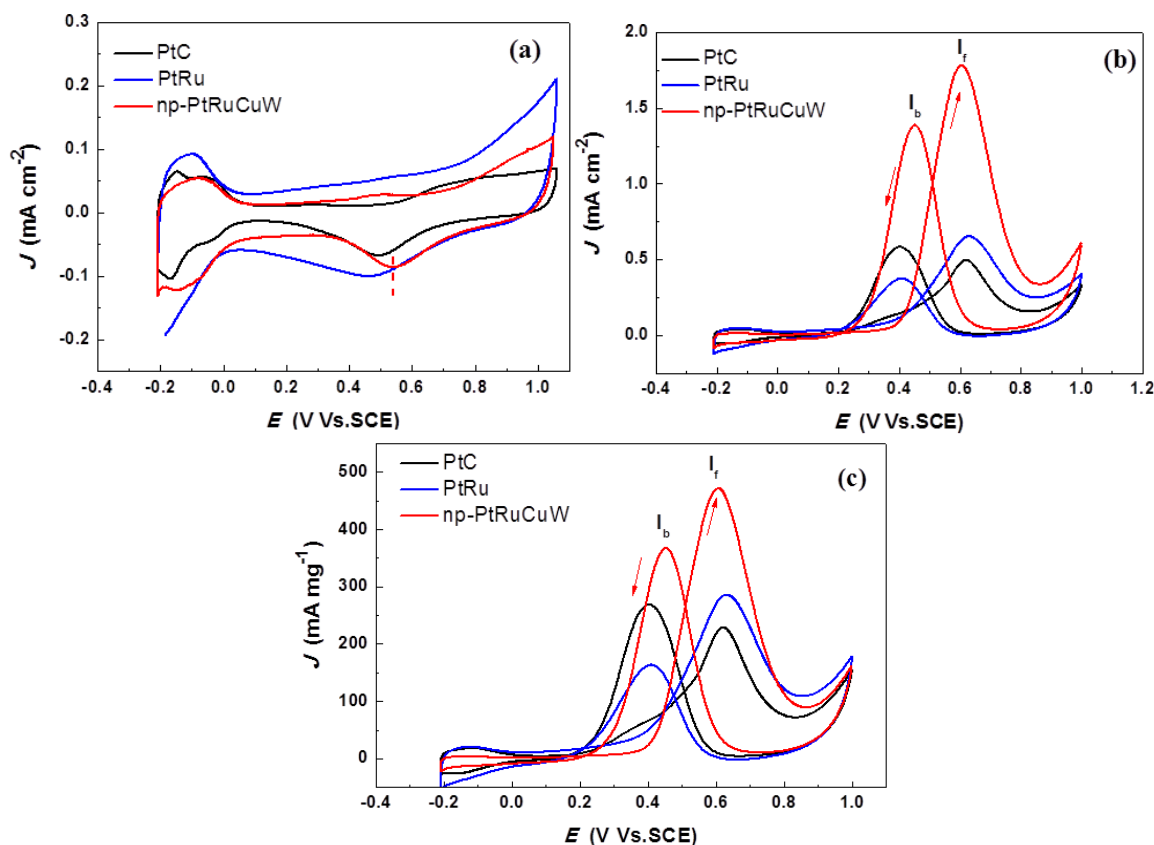

Figure 3. (**a**) The stable CVs of the np-PtRuCuW, PtC and PtRu catalysts in the N₂ purged 0.5 M H₂SO₄ solution (Scan rate: 50 mV s^{-1}); and (**b**) ECSA- and (**c**) mass-normalized activities of the np-PtRuCuW, PtC and PtRu catalysts for methanol oxidation. (Scan rate: 50 mV s^{-1}).

Figure 3b,c shows the ECSA- and Pt mass-normalized results for the np-PtRuCuW, PtC and PtRu catalysts in the H₂SO₄ solution contain 0.5 M CH₃OH. As shown in Figure 3b, the specific activity of the np-PtRuCuW is 1.8 mA cm^{-2}, which is 3.6 and 2.9 times that of the PtC and PtRu catalysts (0.5 and 0.63 mA cm^{-2}), respectively. Further comparison according to Pt mass (Figure 3c) indicates that the np-PtRuCuW catalyst shows higher mass activity of 467.1 mA mg$_{Pt}^{-1}$, which is about 2.0 and 1.6 times of that for PtC and PtRu (229.5 and 287.0 mA mg$_{Pt}^{-1}$). It can be seen that the peak potentials are comparable for all catalysts while the ratio of the forward anodic peak current density (I_f) to the reverse anodic peak current density (I_b) is different. It has been studied that the electro-oxidation of methanol molecules results in the formation of current peak in the forward scan and the removal of the incompletely oxidized carbonaceous species contributes to the current peak in the reverse scan [39]. Hence, the ratio I_f/I_b can be used to measure the tolerance to carbonaceous species [4,36,40]. The values for the np-PtRuCuW, PtC and PtRu are 1.29, 0.91 and

1.75, respectively, which indicates the higher CO tolerance of np-PtRuCuW than PtC while shows disadvantage compared to PtRu.

The subsequent CO tolerance experiment was carried out to characterize our np-PtRuCuW catalyst directly. As shown in Figure 4, the CO stripping peak of np-PtRuCuW (0.47 V *vs.* SCE) is more positive than PtRu catalyst (0.33 V *vs.* SCE). However, there is a remarkable negative shift (about 200 mV) compared to the PtC (0.67 V *vs.* SCE). It is interesting to observe that the stripping curve of np-PtRuCuW presents two CO oxidation peaks, a first peak centered at about 0.47 V (*vs.* SCE) and the second one close to 0.55 V (*vs.* SCE). Moreover, the onset potential for CO stripping is located at around 0.35 V (*vs.* SCE), which is comparable to the peak potential of PtRu. This also suggests the good CO tolerance of our np-PtRuCuW catalyst. Maillard *et al.* [41] observed that catalysts comprising Pt nanoparticles with 2 to 6 nm size exhibited better CO tolerance. Their observations are consistent with our results, which indicate that Pt-based alloys with ligament size of 2.0 ± 0.3 nm have been successfully fabricated.
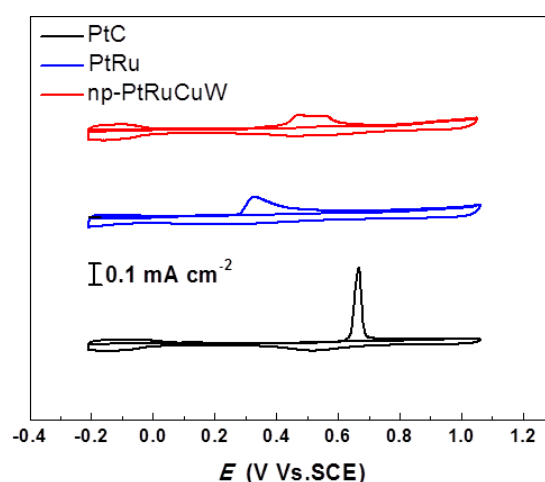

Figure 4. Electrochemical CO-stripping curves of the np-PtRuCuW, PtC and PtRu catalysts in the 0.5 M H_2SO_4 solution (Scan rate: 20 mV s^{-1}).

During the oxidation of methanol on np-PtRuCuW, Pt accomplishes the dissociative chemisorption of methanol and the alloyed metals (Ru, Cu and W) form oxyhydroxide, which extracts an active oxygen to oxidize the carbonaceous residues to CO_2 [42,43]. The three-dimensional bi-continuous structure with interconnected channels and nano-sized ligaments in np-PtRuCuW can facilitate the transportation of molecules and electrons, which greatly improves the reaction kinetics. On the basis of these effects, the present np-PtRuCuW alloy shows superior activity to the commercial PtC and PtRu catalysts. The result also indicates enhanced electrocatalytic performance compared to trimetallic (PtRuCu [27,28] and PtRuW [29,30]).

2.3. Catalytic Activity of np-PtRuCuW towards ORR

Figure 5a displays the CVs of the np-PtRuCuW and PtC catalysts in the N_2-saturated 0.1 M $HClO_4$ solution. Similar to our experiments at anode, the reduction peak of Pt oxides shows a slight positive shift for the np-PtRuCuW catalyst than that of PtC, indicating earlier onset of Pt-O(H) reduction [44,45]. The polarization results for the ORR on the np-PtRuCuW and PtC electrodes are

shown in Figure 5b. It is obvious that the polarization curve of the np-PtRuCuW catalyst shifts to a more positive position than PtC. At cathode, the diffusion-limited region (below 0.8 V *vs.* RHE) suggests a four-electron transfer reaction and indicates low hydrogen peroxide formation [46]. The half-wave potential of the np-PtRuCuW alloy is located at 0.877 V *vs.* RHE, 13 mV positive shift compared to PtC catalyst (0.864 V *vs.* RHE). The present results indicate a greatly enhanced ORR activity of np-PtRuCuW.
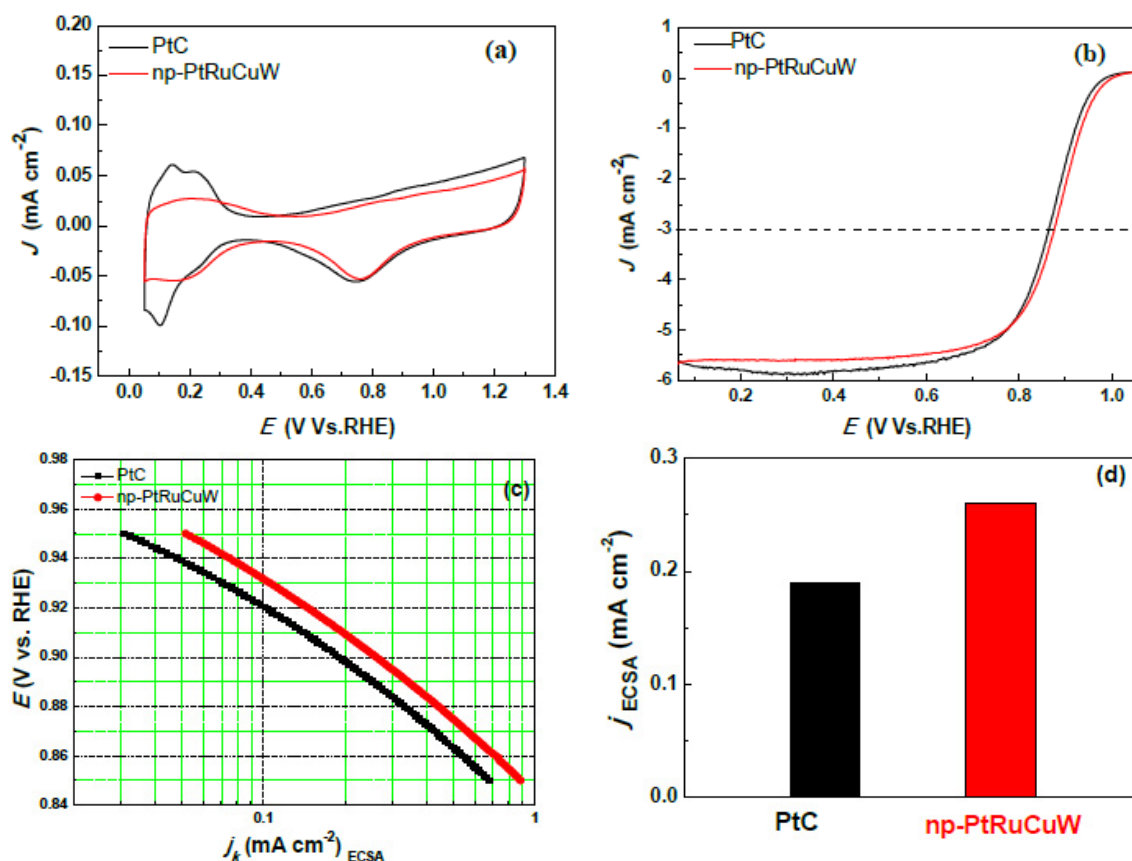

Figure 5. (**a**) CV curves of the np-PtRuCuW and PtC catalysts in the N₂-purged 0.1 M HClO₄ solution (Scan rate: 50 mV s⁻¹); (**b**) ORR results in the O₂-saturated 0.1 M HClO₄ solution at 1600 rpm (Scan rate: 10 mV s⁻¹); (**c**) ECSA-normalized specific kinetic current densities (j_k); and (**d**) the ECSA-normalized specific kinetic current densities for the np-PtRuCuW and PtC catalysts at 0.90 V (*vs.* RHE).

According to the Tafel plots (Figure 5c), the np-PtRuCuW catalyst shows better specific activity than the commercial PtC at the whole selected potential region (0.85~0.95 V *vs.* RHE). Additionally, the Tafel curve of the np-PtRuCuW catalyst is parallel to that of the commercial PtC, which can be observed directly from the plots. This potential region corresponds to ORR when the hydroxyl species (OH$_{ads}$) at Pt active sites and determines the electrode activity. Therefore, the plots demonstrate the similar ORR processes on the np-PtRuCuW and commercial PtC catalysts in acidic media [47,48]. The kinetic current densities at 0.90 V *vs.* RHE represent the activities towards ORR and were calculated by the Koutecky–Levich equation from the ORR polarization curves. The kinetic current densities were normalized by the ECSA to obtain the specific activity in Figure 5d, respectively.

The np-PtRuCuW exhibits a higher specific activity of 0.26 mA cm^{-2}, which is 1.37 times of the commercial PtC catalyst (0.19 mA cm^{-2}).

The ORR consists of four proton and electron transfer ($O_2 + 4H^+ + 4e^- \rightarrow 2H_2O$), O–O breaking and OH_{ads} intermediates formation [46,49]. After alloying with Ru, Cu and W, the lattice parameter of Pt changes which would bring about ligand and strain effects. This will accelerate the scission of the O–O bond and the formation of the OH_{ads}, thus increasing the O_2 reaction rate [50,51]. On the other hand, the hydrogenation rates of OH_{ads} intermediates enhanced and reduced the coverage of Pt surface because of alloy effect [52]. These could rationalize that the present np-PtRuCuW alloy shows improved catalytic performance towards ORR relative to the commercial PtC catalyst.

3. Experimental Section

3.1. Synthesis and Characterizations of np-PtRuCuW

A multi-component $Al_{66}Cu_{30}(Pt_{53}Ru_{32}W_{15})_4$ alloy (nominal composition, at %) was chosen as the precursor and prepared by milling a mixture of pure elemental powders (*i.e.*, Al, Cu, Pt, Ru and W with 99.9 wt. % purity) as before [34,53]. Then, dealloying of the $Al_{66}Cu_{30}(Pt_{53}Ru_{32}W_{15})_4$ alloy powders was carried out in a 1 M HNO_3 solution at room temperature until no obvious bubbles emerged. After the facile dealloying, the samples were rinsed using distilled water and dehydrated alcohol to gain the final np-PtRuCuW catalyst.

X-ray diffractometer (XRD, Rigaku D/max-rB, Osaka, Japan) with Cu Kα radiation was used to analysis the X-ray diffractograms of the $Al_{66}Cu_{30}(Pt_{53}Ru_{32}W_{15})_4$ precursor and as-dealloyed samples. The chemical compositions of the as-dealloyed samples were obtained by an energy-dispersive X-ray (EDX) analyzer in an area-analysis mode (a typical area of 50 μm × 50 μm). Transmission electron microscope (TEM, FEI Tecnai G2, Pleasanton, CA, USA) and high-resolution TEM (HRTEM, FEI Tecnai G2, CA, USA) were also applied to characterize the microstructure. In addition, selected-area electron diffraction (SAED) and fast Fourier transform (FFT) patterns were obtained from the corresponding images.

3.2. Electrochemical Characterization

The ORR and MOR measurements were performed using a standard three-electrode cell with a CHI 760E Potentiostat (CH Instruments, Shanghai, China). The reference electrode was saturated calomel electrode (SCE) and the counter electrode was a bright Pt plate. The catalyst ink preparation and measurement conditions were consistent with our previous report [34,53]. For comparison, we benchmarked the electrochemical properties of the np-PtRuCuW against the commercial (Johnson's Matthey, Pennsylvania, PA, USA) PtC and PtRu catalysts under identical experimental conditions.

4. Conclusions

In conclusion, a novel np-PtRuCuW catalyst has been explored through the combination of a mechanical alloying with the subsequent simple chemical dealloying step. The facile and green technique shows great advantages in the design of multiple component nanostructured alloy electrocatalysts. The np-PtRuCuW catalyst with a unique ligament/channel structure shows enhanced

catalytic activity for methanol oxidation at anode compared to PtC and PtRu catalysts. Furthermore, the catalyst also indicates enhanced catalytic activity towards oxygen reduction reaction at cathode. Our results provide a novel strategy for the design of precursor alloys and fabrication of multi-component nanoporous alloy catalysts for DMFCs.

Acknowledgments

Author Contributions

We thank our collaborators for their contributions to the manuscript. Thank Ying Wang and Qingguo Bai for the fabrication of precursor alloy. Great valuable discussions for the results were supported by Yulai Gao. Xiaoting Chen and Hao Wang carried out most of the experiment and completed documentation and the manuscript. Zhonghua Zhang is in charge of the whole work.

Conflicts of Interest

The authors declare no conflict of interest.

References

1. Kamarudin, S.K.; Achmad, F.; Daud, W.R.W. Overview on the application of direct methanol fuel cell (DMFC) for portable electronic devices. *Int. J. Hyd. Energy* **2009**, *34*, 6902–6916.
2. Zhang, G.; Xia, B.Y.; Wang, X. Strongly Coupled $NiCo_2O_4$-Rgo Hybrid Nanosheets as a Methanol-Tolerant Electrocatalyst for the Oxygen Reduction Reaction. *Adv. Mater.* **2014**, *26*, 2408–2412.
3. Reddington, E.; Sapienza, A.; Gurau, B.; Viswanathan, R.; Sarangapani, S.; Smotkin, E.S.; Mallouk, T.E. Combinatorial electrochemistry: A highly parallel, optical screening method for discovery of better electrocatalysts. *Science* **1998**, *280*, 1735–1737.
4. Ma, X.; Luo, L.; Zhu, L.; Yu, L.; Sheng, L.; An, K.; Ando, Y.; Zhao, X. Pt–Fe catalyst nanoparticles supported on single-wall carbon nanotubes: Direct synthesis and electrochemical performance for methanol oxidation. *J. Power Sour.* **2013**, *241*, 274–280.
5. Wang, C.; Markovic, N.M.; Stamenkovic, V.R. Advanced platinum alloy electrocatalysts for the oxygen reduction reaction. *ACS Catal.* **2012**, *2*, 891–898.
6. Ahmadi, R.; Amini, M.; Bennett, J. Pt–Co alloy nanoparticles synthesized on sulfur-modified carbon nanotubes as electrocatalysts for methanol electrooxidation reaction. *J. Catal.* **2012**, *292*, 81–89.

7. Xu, C.; Hou, J.; Pang, X.; Li, X.; Zhu, M.; Tang, B. Nanoporous PtCo and PtNi alloy ribbons for methanol electrooxidation. *Int. J. Hyd. Energy* **2012**, *37*, 10489–10498.

8. Choi, S.-I.; Xie, S.; Shao, M.; Odell, J.H.; Lu, N.; Peng, H.-C.; Protsailo, L.; Guerrero, S.; Park, J.; Xia, X. Synthesis and characterization of 9 nm Pt–Ni octahedra with a record high activity of 3.3 A/mgPt for the oxygen reduction reaction. *Nano Lett.* **2013**, *13*, 3420–3425.

9. Cui, C.; Gan, L.; Heggen, M.; Rudi, S.; Strasser, P. Compositional segregation in shaped Pt alloy nanoparticles and their structural behaviour during electrocatalysis. *Nat. Mater.* **2013**, *12*, 765–771.

10. Zhang, X.; Li, D.; Dong, D.; Wang, H.; Webley, P.A. One-step fabrication of ordered Pt–Cu alloy nanotube arrays for ethanol electrooxidation. *Mater. Lett.* **2010**, *64*, 1169–1172.

11. Sun, S.; Zhang, G.; Geng, D.; Chen, Y.; Banis, M.N.; Li, R.; Cai, M.; Sun, X. Direct growth of single-crystal Pt nanowires on Sn@CNT nanocable: 3D electrodes for highly active electrocatalysts. *Chem. A Eur. J.* **2010**, *16*, 829–835.

12. Zou, L.; Guo, J.; Liu, J.; Zou, Z.; Akins, D.L.; Yang, H. Highly alloyed PtRu black electrocatalysts for methanol oxidation prepared using magnesia nanoparticles as sacrificial templates. *J. Power Sources.* **2014**, *248*, 356–362.

13. Guo, J.; Zhao, T.; Prabhuram, J.; Chen, R.; Wong, C. Preparation and characterization of a PtRu/C nanocatalyst for direct methanol fuel cells. *Electrochim. Acta* **2005**, *51*, 754–763.

14. Lipkowski, J.; Ross, P.N. *Electrocatalysis*; John Wiley & Sons: New York, NY, USA, 1998; Volume 3, pp. 70–200.

15. Kua, J.; Goddard, W.A. Oxidation of methanol on 2nd and 3rd row group viii transition metals (Pt, Ir, Os, Pd, Rh, and Ru): Application to direct methanol fuel cells. *J. Am. Chem. Soc.* **1999**, *121*, 10928–10941.

16. Tong, Y.; Rice, C.; Wieckowski, A.; Oldfield, E. A detailed NMR-based model for CO on Pt catalysts in an electrochemical environment: Shifts, relaxation, back-bonding, and the Fermi-Level local density of states. *J. Am. Chem. Soc.* **2000**, *122*, 1123–1129.

17. Zhou, W.; Zhou, Z.; Song, S.; Li, W.; Sun, G.; Tsiakaras, P.; Xin, Q. Pt based anode catalysts for direct ethanol fuel cells. *Appl. Catal. B* **2003**, *46*, 273–285.

18. Liu, H.; Song, C.; Zhang, L.; Zhang, J.; Wang, H.; Wilkinson, D.P. A review of anode catalysis in the direct methanol fuel cell. *J. Power Sour.* **2006**, *155*, 95–110.

19. Liu, Z.; Lee, J.Y.; Han, M.; Chen, W.; Gan, L.M. Synthesis and characterization of PtRu/C catalysts from microemulsions and emulsions. *J. Mater. Chem.* **2002**, *12*, 2453–2458.

20. Almeida, T.; Palma, L.; Leonello, P.; Morais, C.; Kokoh, K.; de Andrade, A. An optimization study of PtSn/C catalysts applied to direct ethanol fuel cell: Effect of the preparation method on the electrocatalytic activity of the catalysts. *J. Power Sour.* **2012**, *215*, 53–62.

21. Liu, L.; Huang, Z.; Wang, D.; Scholz, R.; Pippel, E. The fabrication of nanoporous Pt-based multimetallic alloy nanowires and their improved electrochemical durability. *Nanotechnology* **2011**, *22*, 105604, doi:10.1088/0957-4484/22/10/105604.

22. Chen, Z.; Waje, M.; Li, W.; Yan, Y. Supportless Pt and PtPd nanotubes as electrocatalysts for oxygen-reduction reactions. *Angew. Chem. Int. Ed.* **2007**, *46*, 4060–4063.

23. You, T.; Niwa, O.; Tomita, M.; Hirono, S. Characterization of platinum nanoparticle-embedded carbon film electrode and its detection of hydrogen peroxide. *Anal. Chem.* **2003**, *75*, 2080–2085.

24. Weissmüller, J.; Viswanath, R.; Kramer, D.; Zimmer, P.; Würschum, R.; Gleiter, H. Charge-induced reversible strain in a metal. *Science* **2003**, *300*, 312–315.

25. Qi, Z.; Geng, H.; Wang, X.; Zhao, C.; Ji, H.; Zhang, C.; Xu, J.; Zhang, Z. Novel nanocrystalline PdNi alloy catalyst for methanol and ethanol electro-oxidation in alkaline media. *J. Power Sour.* **2011**, *196*, 5823–5828.

26. Xu, C.; Liu, Y.; Hao, Q.; Duan, H. Nanoporous PdNi alloys as highly active and methanol-tolerant electrocatalysts towards oxygen reduction reaction. *J. Mater. Chem. A* **2013**, *1*, 13542–13548.

27. Jeon, M.K.; Cooper, J.S.; McGinn, P.J. Methanol electro-oxidation by a ternary Pt–Ru–Cu catalyst identified by a combinatorial approach. *J. Power Sour.* **2008**, *185*, 913–916.

28. Naidoo, Q.-L.; Naidoo, S.; Petrik, L.; Nechaev, A.; Ndungu, P.; Vaivars, G. Synthesis highly active platinum tri-metallic electrocatalysts using "one-step" organometallic chemical vapour deposition technique for methanol oxidation process. *IOP Conf. Ser. Mater. Sci. Eng.* **2012**, doi:10.1088/1757-899X/38/1/012031.

29. Kang, D.K.; Noh, C.S.; Park, S.T.; Sohn, J.M.; Kim, S.K.; Park, Y.-K. The effect of PtRuW ternary electrocatalysts on methanol oxidation reaction in direct methanol fuel cells. *Korean J. Chem. Eng.* **2010**, *27*, 802–806.

30. Jeon, M.K.; Lee, K.R.; Woo, S.I. Ternary $Pt_{45}Ru_{45}M_{10}$/C (M = Mn, Mo and W) catalysts for methanol and ethanol electro-oxidation. *Korean J. Chem. Eng.* **2009**, *26*, 1028–1033.

31. Aricò, A.S.; Antonucci, P.L.; Modica, E.; Baglio, V.; Kim, H.; Antonucci, V. Effect of PtRu alloy composition on high-temperature methanol electro-oxidation. *Electrochim. Acta* **2002**, *47*, 3723–3732.

32. Ammam, M.; Easton, E.B. Quaternary PtMnCuX/C (X = Fe, Co, Ni, and Sn) and PtMnMoX/C (X = Fe, Co, Ni, Cu and Sn) alloys catalysts: Synthesis, characterization and activity towards ethanol electrooxidation. *J. Power Sour.* **2012**, *215*, 188–198.

33. Qian, L.; Chen, M. Ultrafine nanoporous gold by low-temperature dealloying and kinetics of nanopore formation. *Appl. Phys. Lett.* **2007**, *91*, 083105, doi:10.1063/1.2773757.

34. Chen, X.; Jiang, Y.; Sun, J.; Jin, C.; Zhang, Z. Highly active nanoporous Pt-based alloy as anode and cathode catalyst for direct methanol fuel cells. *J. Power Sour.* **2014**, *267*, 212–218.

35. Pozio, A.; de Francesco, M.; Cemmi, A.; Cardellini, F.; Giorgi, L. Comparison of high surface Pt/C catalysts by cyclic voltammetry. *J. Power Sour.* **2002**, *105*, 13–19.

36. Lee, Y.-W.; Ko, A.-R.; Han, S.-B.; Kim, H.-S.; Park, K.-W. Synthesis of octahedral Pt–Pd alloy nanoparticles for improved catalytic activity and stability in methanol electrooxidation. *Phys. Chem. Chem. Phys.* **2011**, *13*, 5569–5572.

37. Li, H.H.; Cui, C.H.; Zhao, S.; Yao, H.B.; Gao, M.R.; Fan, F.J.; Yu, S.H. Mixed-PtPd-shell PtPdCu nanoparticle nanotubes templated from copper nanowires as efficient and highly durable electrocatalysts. *Adv. Energy Mater.* **2012**, *2*, 1182–1187.

38. He, C.; Liang, Y.; Fu, R.; Wu, D.; Song, S.; Cai, R. Nanopores array of ordered mesoporous carbons determine Pt's activity towards alcohol electrooxidation. *J. Mater. Chem.* **2011**, *21*, 16357–16364.

39. Mancharan, R.; Goodenough, J.B. Methanol oxidation in acid on ordered NiTi. *J. Mater. Chem.* **1992**, *2*, 875–887.

40. Xu, C.; Wang, L.; Wang, R.; Wang, K.; Zhang, Y.; Tian, F.; Ding, Y. Nanotubular mesoporous bimetallic nanostructures with enhanced electrocatalytic performance. *Adv. Mater.* **2009**, *21*, 2165–2169.

41. Maillard, F.; Schreier, S.; Hanzlik, M.; Savinova, E.R.; Weinkauf, S.; Stimming, U. Influence of particle agglomeration on the catalytic activity of carbon-supported Pt nanoparticles in Co monolayer oxidation. *Phys. Chem. Chem. Phys.* **2005**, *7*, 385–393.

42. Ley, K.L.; Liu, R.; Pu, C.; Fan, Q.; Leyarovska, N.; Segre, C.; Smotkin, E. Methanol oxidation on single-phase Pt-Ru-Os ternary alloys. *J. Electrochem. Soc.* **1997**, *144*, 1543–1548.

43. Lei, H.-W.; Suh, S.; Gurau, B.; Workie, B.; Liu, R.; Smotkin, E.S. Deuterium isotope analysis of methanol oxidation on mixed metal anode catalysts. *Electrochim. Acta* **2002**, *47*, 2913–2919.

44. Zhang, X.; Choi, I.; Qu, D.; Wang, L.; Lee, C.-W.J. Coverage-dependent electro-catalytic activity of Pt sub-monolayer/Au bi-metallic catalyst toward methanol oxidation. *Int. J. Hyd. Energy* **2013**, *38*, 5665–5670.

45. Hodnik, N.; Jeyabharathi, C.; Meier, J.C.; Kostka, A.; Phani, K.L.; Rečnik, A.; Bele, M.; Hočevar, S.; Gaberšček, M.; Mayrhofer, K.J. Effect of ordering of $PtCu_3$ nanoparticle structure on the activity and stability for the oxygen reduction reaction. *Phys. Chem. Chem. Phys.* **2014**, *16*, 13610–13615.

46. Stephens, I.E.L.; Bondarenko, A.S.; Grønbjerg, U.; Rossmeisl, J.; Chorkendorff, I. Understanding the electrocatalysis of oxygen reduction on platinum and its alloys. *Energy Environ. Sci.* **2012**, *5*, 6744–6762.

47. Hu, Y.; Jensen, J.O.; Zhang, W.; Cleemann, L.N.; Xing, W.; Bjerrum, N.J.; Li, Q. Hollow spheres of iron carbide nanoparticles encased in graphitic layers as oxygen reduction catalysts. *Angew. Chem. Int. Ed.* **2014**, *53*, 3675–3679.

48. Kongkanand, A.; Kuwabata, S.; Girishkumar, G.; Kamat, P. Single-wall carbon nanotubes supported platinum nanoparticles with improved electrocatalytic activity for oxygen reduction reaction. *Langmuir* **2006**, *22*, 2392–2396.

49. Guo, S.; Zhang, S.; Sun, S. Tuning nanoparticle catalysis for the oxygen reduction reaction. *Angew. Chem. Int. Ed.* **2013**, *52*, 8526–8544.

50. Toda, T.; Igarashi, H.; Uchida, H.; Watanabe, M. Enhancement of the electroreduction of oxygen on Pt alloys with Fe, Ni, and Co. *J. Electrochem. Soc.* **1999**, *146*, 3750–3756.

51. Toda, T.; Igarashi, H.; Watanabe, M. Role of electronic property of Pt and Pt alloys on electrocatalytic reduction of oxygen. *J. Electrochem. Soc.* **1998**, *145*, 4185–4188.

52. Zhang, J.; Vukmirovic, M.B.; Xu, Y.; Mavrikakis, M.; Adzic, R.R. Controlling the catalytic activity of platinum-monolayer electrocatalysts for oxygen reduction with different substrates. *Angew. Chem. Int. Ed.* **2005**, *44*, 2132–2135.

53. Chen, X.; Si, C.; Gao, Y.; Frenzel, J.; Sun, J.; Eggeler, G.; Zhang, Z. Multi-component nanoporous platinum-ruthenium-copper-osmium-iridium alloy with enhanced electrocatalytic activity towards methanol oxidation and oxygen reduction. *J. Power Sour.* **2015**, *273*, 324–332.